Non-Drude Behavior in Indium-Tin-Oxide Nanowhiskers and Thin Films Investigated by Transmission and Reflection THz Time-Domain Spectroscopy

Chan-Shan Yang, Mao-Hsiang Lin, Chia-Hua Chang, Peichen Yu, *Member, IEEE*, Jia-Min Shieh, Chang-Hong Shen, Osamu Wada, *Fellow, IEEE*, and Ci-Ling Pan, *Fellow, IEEE*

***Abstract*— A comparative study of indium-tin-oxide (ITO) nanowhiskers (NWhs) and thin films as transparent conductors in the terahertz frequency range are conducted. We employ both transmission-type and reflection-type terahertz time-domain spectroscopies (THz-TDTS and THz-TDRS) to explore the far-infrared optical properties of these samples. Their electrical properties, such as plasma frequencies and carrier scattering times, are analyzed and found to be fitted well by the Drude-Smith model over 0.1–1.4 THz. Further, structural and crystalline properties of samples are examined by scanning electron microscopy and X-ray diffraction, respectively. Non-Drude behavior of complex conductivities in ITO NWhs is attributed to carrier scattering from grain boundaries and impurity ions. In ITO thin films, however, the observed non-Drude behavior is ascribed to scattering by impurity ions only. Considering NWhs and thin films with the same height, mobility of the former is $\sim$125 $cm^2\ V^{-1}s^{-1}$, much larger than those of the ITO thin films, $\sim$27 $cm^2\ V^{-1}s^{-1}$. This is attributed to the longer carrier scattering time of the NWhs. The dc conductivities ($\sim$250 $\Omega^{-1}cm^{-1}$) or real conductivities in the THz frequency region of ITO NWhs is, however, lower than those of the ITO thin films ($\sim$800 $\Omega^{-1}cm^{-1}$) but adequate for use as electrodes. Partly, this is a reflection of the much higher plasma frequencies of thin films. Significantly, the transmittance of ITO NWhs ($\cong$ 60%–70%) is much higher ($\cong$ 13 times) than those of ITO thin films in the THz frequency range. The underneath basic physics is that the THz radiation can easily propagate through the air-space among NWhs. The superb transmittance and adequate electrical properties of ITO NWhs suggest their potential applications as transparent conducting electrodes in THz devices.**

***Index Terms*— Complex conductivity, dielectric function, drude-smith model, effective medium theory, far infrared, indium tin oxide, nanomaterial, optical constants, scattering time, spectroscopy, terahertz.**

I. Introduction

INDIUM-TIN-OXIDE (ITO), an n-type semiconductor, has been one of the most frequently used transparent conducting oxides (TCOs). This is due to its wide band gap and relatively high electrical conductivity [1], [2]. To date, ITO thin films have been widely employed as transparent electrodes and direct-Ohmic contact structures in optoelectronic devices, e.g., light emitting diodes (LED) [3], [4], solar cells [5], liquid crystal displays (LCD) [6], [7], optical disk cavities [8], biosensor [9], optical pulse shapers [10], and fiber refractometers [11]. As a result, optical and electrical characteristics of ITO thin films have been extensively investigated [12]−[15]. The most important material properties of ITO thin films are their high average transmission (>92%) in the visible band [14], and low resistivity (<200 $\mu\Omega$·cm) [12], [14]. In recent years, ITO nanocolumns, e.g., nanorods, nanopillars, nanowires (NWs) and nanowhiskers (NWhs), have aroused great interests because of their excellent electrical characteristics as well as broadband and omnidirectional anti-reflection (AR) properties in the visible region [16]−[18]. In general, the resistivity of individual ITO nanocolumns ranges from 100 $\mu\Omega$·cm to several thousands of $\mu\Omega$·cm at room-temperature [19]. Their transmittance can be higher than 95% in the visible range [20], [21]. A number of groups have reported electrical and optical characteristics of ITO nanocolumns [19], [20], [22], [23]. However, there are some shortcomings in these previous measurements of electrical properties of ITO nanomaterials. First of all, a measurement by the scanning probe provides information on individual nanocolumns instead of shedding lights on behavior of carriers over an area. The latter is relevant for device applications. Conventional Hall measurement, on the other hand, is destructive because it requires making electrical contacts on the nanostructures or thin films [19], [22]. Finally, the measurement at lower frequencies can only probe the macroscopically

Manuscript received March 18, 2013; revised June 1, 2013; accepted June 13, 2013. Date of publication June 25, 2013; date of current version July 2, 2013. This work was supported by the National Science Council in Taiwan under Grant 101-2221-E-007-103-MY3 and the Academic Top University Program of the Ministry of Education.

C.-S. Yang and M.-H. Lin are with the Department of Physics, National Tsing Hua University, Hsinchu 30013, Taiwan (e-mail: yangchanshan@gmail.com; smanax@gmail.com).

C.-H. Chang and P. Yu are with the Department of Photonics and Institute of Electro-Optical Engineering, National Chiao Tung University, Hsinchu 30010, Taiwan (e-mail: nctueric@gmail.com; yup@faculty.nctu.edu.tw).

J.-M. Shieh is with the National Nano Devices Laboratories, Hsinchu 30078, Taiwan, and also with the Department of Photonics, Institute of Electro-Optical Engineering, National Chiao Tung University, Hsinchu 30010, Taiwan (e-mail: jmshieh@ndl.narl.org.tw).

C.-H. Shen is with the National Nano Devices Laboratories, Hsinchu 30078, Taiwan (e-mail: chshen@ndl.narl.org.tw).

O. Wada is with the Center for Collaborative Research and Technology Development, Kobe University, Kobe 657-8501, Japan (e-mail: owada@kobe-u.ac.jp).

C.-L. Pan is with the Department of Physics, National Tsing Hua University, Hsinchu 30013, Taiwan, and also with the Institute of Photonics Technologies and the Frontier Research Center on Fundamental and Applied Science of Matters, Tsukuba 305-8565, Japan (e-mail: clpan@phys.nthu.edu.tw).

Color versions of one or more of the figures in this paper are available online at http://ieeexplore.ieee.org.

Digital Object Identifier 10.1109/JQE.2013.2270552

electrical properties, instead of the nanometer length-scale range, which is close to the grain sizes of typical nanostructured material and corresponding to the terahertz (THz) region by considering the diffusion coefficient [24].

What is more, in consideration of the growing demand of THz optoelectronic devices [25], it is natural to explore applications of ITO in the far-infrared wavelength range. Several millimeter wave and THz devices employing ITO thin films have been reported [26]−[29]. Therefore, a complete understanding of the far-infrared optical and electrical properties of ITO materials is requisite. Fourier transform infrared spectroscopy (FTIR) has been one of the popular methods employed to determine the optical and electrical properties of conducting films [30], [31]. Lately, THz time-domain spectroscopy (THz-TDS) has also been widely used for investigating the optical and electrical parameters of a wide-range of materials relevant to our work, e.g., thin metal films [32], epilayers [33], bulk semiconductor [34], and several kinds of nanostructures [35]−[46]. The transmittance and complex optical constants of ITO thin films by transmission-type THz-TDS (THz-TDTS) were reported [29], [47]. In our previous study, we employed the Drude model to deduce the complex conductivities and other relevant electrical parameters of sputtered ITO thin films also by THz-TDTS [31]. However, the appropriateness of the Drude model here can be argued because of slightly negative values of the imaginary conductivities of ITO films [31]. Recently, we have reported the optical and electrical properties of ITO bottom layer atop the substrate of ITO NWhs [48]. Such a layer exhibits excellent crystallinity with large grain size, strong back scattering effect at domain walls and complete carrier localization in the NWhs. Unfortunately, this particular nanostructured sample is somewhat non-uniform and the structures of ITO NWhs consist of trunks with many branches. As a result, the complex optical and electrical properties in the direction of electrical field parallel to the branches can be affected by the more complex structure [48]. On the other hand, taking the far-infrared characteristics of ITO materials, i.e., the high reflectance and strong absorption [30], [31] into account, it is desirable to conduct also reflection-type THz-TDS (THz-TDRS) measurements to confirm the accuracy and reliability of material parameters extracted from THz-TDTS data. Further, ITO nanostructures are frequently deposited on silicon or fused silica substrates that can be over 500∼1000 times thicker than the heights of nanostructures. Due to the larger phase change induced by much more thicker substrates than nanostructures, THz-TDTS might not be able to offer enough sensitivity for extraction of accurate optical constants [49]. Indeed, THz-TDRS has been applied to study metals [50], [51], superconductors [50], [52], highly doped silicon [53], the explosive RDX [54], and aqueous alcohol [55] for the above reasons. To our knowledge, there has been no previous study of TCO nanostructures by using THz-TDRS. Furthermore, the information on reflective response of ITO nanostructure is important for designing the optoelectronic devices in THz frequency range.

In this work, ITO NWhs and thin films were prepared by the glancing-angle electron-beam evaporation method and direct current (DC) reactive magnetron sputtering methods, respectively. The transmittance and reflectance of both types of samples were determined. The frequency-dependent complex conductivities, refractive indices and extinction coefficients of the ITO NWhs and thin films have also been investigated by employing both THz-TDTS and THz-TDRS. The model of a thin film in the effective medium approximation (EMA) was employed to analyze the nanostructures in the THz frequency range [38], [56]. Electrical properties of the ITO nanostructures and thin films, such as plasma frequency (ω_p), carrier scattering time (τ), mobility (μ), and carrier concentration (N_e), were extracted by using the Drude-Smith model [57]. This model takes into account carrier localization and is widely used to describe non-Drude-like behavior in poor conductors and nanostructured materials [35]−[37], [39], [40], [46], [58]. Regarding ITO NWhs, the effect of the grain boundary on carrier transport cannot be ignored because of their mean free paths are comparable to the grain size [59]. For ITO thin films fabricated by the method of sputtering, however, it is shown that backscattering of carriers by impurity ions is the dominant mechanism for the localization of carriers.

This paper is organized as follows. In Section II, we introduce the preparation and structural characteristics of the ITO NWhs and thin films. The experimental setups for THz spectroscopic studies are described briefly. The method of extracting the optical and electrical parameters of the samples from THz-TDS will also be presented. In Section III, we show the experimental results and their analysis Finally, we summarize conclusions of this study in Section IV.

II. Experimental and Theoretical Methods

A. Preparation and Characterization of the ITO Nanowhiskers and ITO Thin Films

By applying glancing angle electron-beam evaporation, ITO NWhs can be deposited on (100)-oriented silicon substrates of high resistivity. The target source for deposition was the oxide material composed of 5% SnO_2 and 95% In_2O_3. The double-side-polished silicon substrate was attached to a holder, which was tilted at a deposition angle of 70° with respect to the incident vapor flux. At the beginning of the evaporation, the pressure was pumped down to $\sim 10^{-6}$ torr in the chamber. During growth, the chamber was stabilized at 280 °C and a vacuum of $\sim 10^{-4}$ torr was maintained. In order to observe the growth status of ITO NWhs, we set the deposition time of samples at either 11 min. or 22 min., with a deposition rate of 0.15 nm per second.

The ITO NWhs were characterized by scanning electron microscopy (SEM, JEOL 7000). Figure 1 shows the SEM images of the ITO NWhs with deposition times of (a) 11 minutes and (b) 22 minutes. The tilted top views of the NWhs are shown in Fig. 1(a) and Fig. 1(b), respectively. The corresponding cross-sectional images of the NWhs are shown in Fig. 1(c) and 1(d). The heights of ITO NWhs are estimated to be 431.2 nm (short NWhs) and 1387.7 nm (long NWhs). We observed side branches starting to grow along the sides of ITO trunk after nanorods become longer than 1 μm.

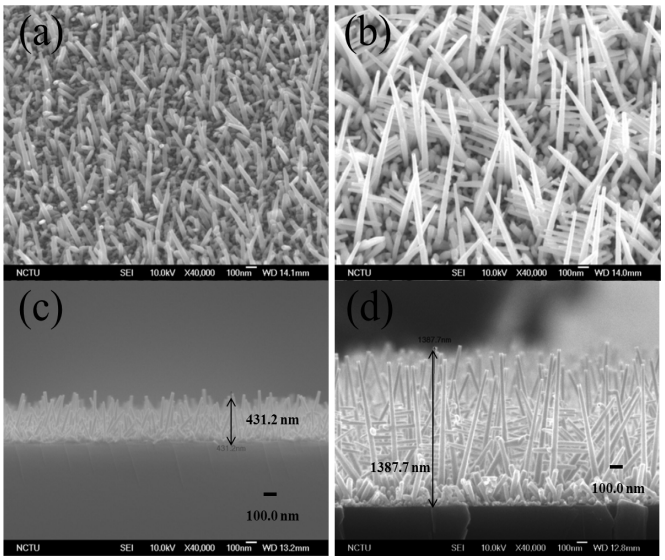

Fig. 1. The scanning electron microscopic images of the ITO NWhs fabricated with deposition times of (a) 11 minutes (b) 22 minutes. The corresponding cross-sectional images in (c) and (d) show the estimated heights of 431.2 nm (short NWhs) and 1387.7 nm (long NWhs), respectively.

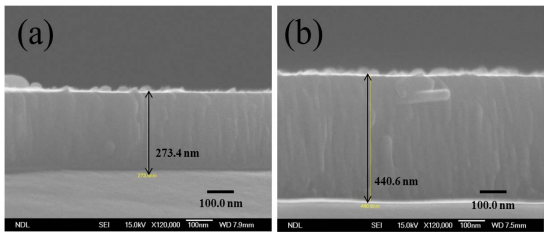

Fig. 2. The scanning electron microscopic cross-sectional images of the ITO thin films show these two samples have estimated heights of (a) 273.4 nm and (b) 440.6 nm, respectively.

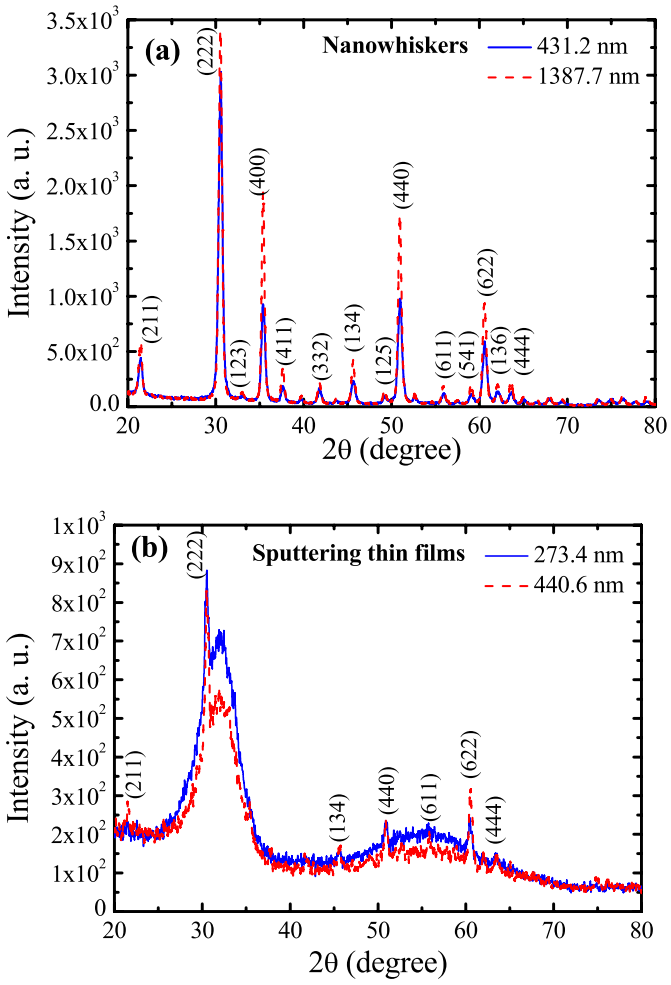

Fig. 3. X-ray diffraction patterns for (a) ITO NWhs and (b) ITO thin films. In Fig. 3(a), the blue solid line and red dash line correspond to ITO NWhs with heights of 431.2 nm (short NWhs) and 1387.7 nm (long NWhs), respectively. In Fig. 3(b), the blue and red solid lines correspond to ITO thin films with heights of 273.4 nm and 440.6 nm, respectively.

The ITO thin films were fabricated by DC reactive magnetron sputtering. The target was composed of 5% SnO_2 and 95% In_2O_3, which was the same condition for depositing ITO NWhs. The sputtering power was set at 300 W. Argon (20 sccm) and oxygen (0.4 sccm) were injected into the chamber and fixed at the total pressure of $\sim 10^{-5}$ torr. The substrates were kept at a fixed temperature of 20 °C. The cross-sectional views of ITO thin films are shown in Fig. 2(a) and Fig. 2(b), respectively. The heights of films are determined to be (a) 273.4 nm and (b) 440.6 nm, respectively.

In addition, the crystalline quality of the ITO NWhs and ITO thin films were characterized by X-ray diffraction (XRD, PANalytical X'Pert Pro, MRD) with high resolution at the incident angle of 0.5 degree. The X-ray radiation source applied was Cu K_α radiation with wavelength of 0.154 nm. Figure 3 shows the XRD patterns for ITO NWhs of different heights and thin films, respectively. Examining Fig. 3(a), we find that the ITO NWhs have a <111> preferred orientation because the intensity of the (222) peak is stronger than others. The samples of NWhs with two different deposition times exhibit similar crystal structures. Intensity ratios of the (222) and (400) diffraction peaks for 431.2nm- and 1387.7nm-high NWhs are 3.28 and 1.72, respectively. The full-width-at-half maximum (FWHM) of a peak in XRD patterns is related to the average grain size of the material under investigation. By applying the Scherrer formula [60], given by $G = 0.93 \cdot \lambda / (\text{FWHM} \times \cos\theta)$, where G is the average grain size, θ is angular position of the diffraction peak and λ is the wavelength of the X-ray radiation used, we find the crystal grain sizes of (222) orientation of ITO short and long NWhs are 17.36 nm and 19.40 nm, respectively. This trend is consistent with similar analysis of the (400) peak, which yield crystal grain sizes of 18.23 nm and 22.46 nm, respectively for the above mentioned samples. The above XRD analysis reveals that ITO NWhs prefer to grow along the plane [100] under a low-oxygen environment. In contrast, XRD pattern of ITO thin films reveal strongly amorphous characteristics with no preferred orientation (see Fig. 3(b)). Note also the broader linewidth of the XRD peaks for ITO thin films than NWhs. This is further proof that the NWhs exhibit better crystalline quality than the films.

B. Experimental Setups for THz-TDTS and THz-TDRS

Two photoconductive (PC) antenna-based THz-TDS as described in our previous works were used to characterize

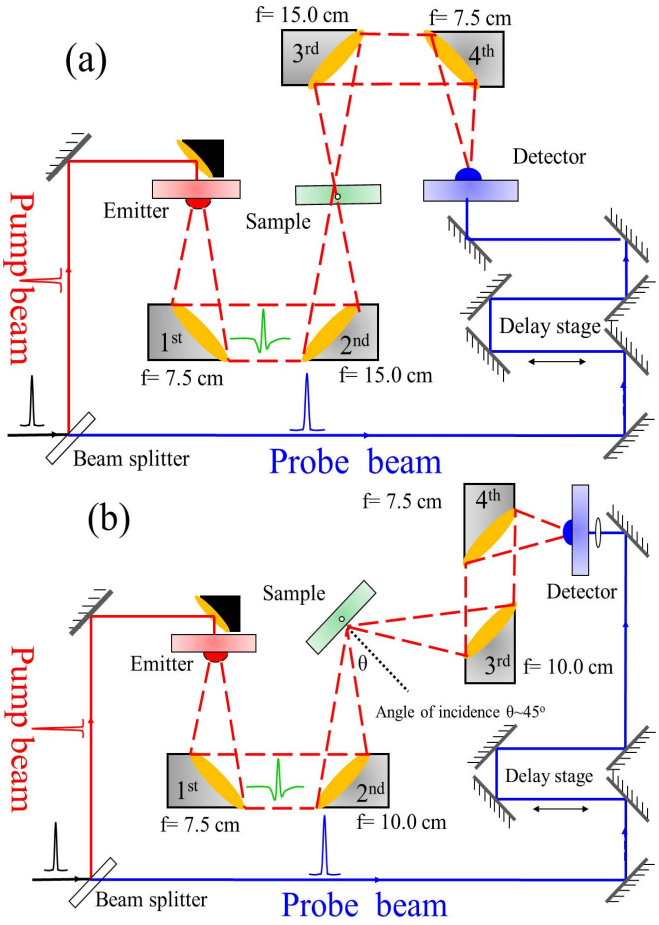

Fig. 4. Schematic drawings of the homemade (a) transmission and (b) reflection type THz-TDS. The exciting and probing pulses are from a femtosecond Ti: Sapphire laser. The emitters and detectors are photoconductive antennas.

the samples in the frequency range between 100 GHz and 1.6 THz [48], [61]–[63]. The schematic diagram of our THz-TDTS is shown in Fig. 4(a). Two pairs of symmetrically placed parabolic mirrors with focal lengths of 7.5 and 15 cm were employed. Their diameters of long versus short axis are 7 versus 5 cm, and 10 versus 7 cm, respectively. The dynamic range of our THz-TDTS is as high as 10^6. The experimental setup of the THz-TDRS is shown in Fig. 4(b). The focal lengths of the two pairs of symmetrically placed parabolic mirrors are 7.5 and 10 cm. All diameters of long and short axis are 7 and 5 cm, respectively. The dynamic range of this system is $\sim 10^{5.5}$. The radius of the THz beam at the sample position is around 5 mm, while the angle of incidence (AOI) of the THz beam on the target is ~45°. During measurements, both systems are purged with nitrogen at a relative humidity of 4.5 ± 0.5%.

C. Determination of THz Optical Constants by THz-TDTS and THz-TDRS

In the THz frequency range, if the heights of measured nanostructures are only several micrometers or hundred nanometers, subsequent THz signals caused by the multi-reflections from the interfaces cannot be separated from the main peak in the time domain. Therefore, the effect should be considered in the analytic model for both systems.

In our previous work [48], the ITO NWhs were of low density and not uniformly distributed. We treated such samples as a kind of graded-refractive-index structure instead of the uniform film. Such a profile of complex refractive indices has to be supposed in order to match observed low reflectance of such samples with respect to the sputtered ITO film. Samples of NWhs in this study, however, show uniform trunks and branches with high density. Therefore, the ITO NWhs in this work are modeled by the thin film model within the effective medium approximation (EMA).

We consider a monochromatic plane THz wave propagating through the sample on the substrate at normal incidence [31]. Further, the slight difference in thickness of substrates of the sample and reference is taken into account by Δd. The complex transmission coefficient of the nanostructure (or thin film), normalized to that of the bare substrate, can be written as [64],

$$\begin{aligned} T^*_{Theo,0^\circ}(\omega) &= E^*_{Sam,T}(\omega)/E^*_{Ref,T}(\omega) \\ &= t^*_{12,0^\circ}\cdot t^*_{23,0^\circ}\cdot \exp\left[i\cdot\left(n_2^*-1\right)\cdot d\cdot\omega/c\right] \\ &\quad \Big/ \left\{ \begin{array}{l} t^*_{13,0^\circ}\cdot\left[1-r^*_{23,0^\circ}\cdot r^*_{21,0^\circ}\cdot\exp\left(i\cdot 2n_2^*\cdot d\cdot\omega/c\right)\right] \\ \cdot\exp\left[i\cdot\left(n_3^*-1\right)\cdot\Delta d\cdot\omega/c\right] \end{array} \right\}, \end{aligned} \tag{1}$$

where $E^*_{Sam,T}(\omega)$ and $E^*_{Ref,T}(\omega)$ are electric fields of the THz wave transmitted through the sample and the bare substrate, respectively; $t^*_{12,0^\circ}$, $t^*_{23,0^\circ}$ and $t^*_{13,0^\circ}$ are the transmission coefficients of the THz signal at the normal incidence (0°) from air (medium #1) to the nanostructure or thin film (medium #2), from the nanostructure or thin film to the substrate (medium #3), and from air to the substrate, respectively. Similarly, $r^*_{23,0^\circ}$ and $r^*_{21,0^\circ}$ are the reflection coefficients of the THz signal at normal incidence from the nanostructure (or thin film) to the substrate, and from the nanostructure (or thin film) to air, respectively. Here, n_2^* and n_3^* are the equivalent refractive indices of the nanostructure (or thin film) and the substrate, respectively. Additionally, d is the height of the nanostructure (or thin film); ω and c are the angular frequency and speed of light in vacuum, respectively.

In THz-TDRS, we can also write the complex reflection coefficient of the nanostructure (or thin film), normalized to that of the bare substrate [64], as

$$\begin{aligned} R^*_{Theo,45^\circ}(\omega) &= E^*_{Sam,R}/E^*_{Ref,R} \\ &= \left\{ \begin{array}{l} \left[r^*_{12,45^\circ}+r^*_{23,45^\circ}\cdot\exp\left(i\cdot 2\delta\right)\right]/ \\ \left[1+r^*_{12,45^\circ}\cdot r^*_{23,45^\circ}\cdot\exp\left(i\cdot 2\delta\right)\right] \end{array} \right\}\cdot\exp\left(i\pi\right), \end{aligned} \tag{2}$$

where $\delta = \omega\cdot n_2^*\cdot d/(\cos\theta_2\cdot c)$ is the phase difference experienced by the THz wave propagating through the sample; $E^*_{Sam,R}(\omega)$ and $E^*_{Ref,R}(\omega)$ are the electric fields of the THz wave reflected from the sample and reference, i.e., bare substrate, respectively. The parameters, $r^*_{12,45^\circ}$ and $r^*_{23,45^\circ}$, are the reflection coefficients of air-nanostructure (or thin film) and nanostructure (or thin film)-substrate interfaces at AOI = 45° , respectively. By considering the THz field with p-polarization, the ratio $r^*_{12,45^\circ}$ and $r^*_{23,45^\circ}$ can be defined.

Experimentally, the transmission coefficient $T^*_{Exp,0^\circ}(\omega)$ and reflection coefficient $R^*_{Exp,45^\circ}(\omega)$ are determined from the ratios of the transmitted and reflected THz signals, respectively. Finally, we define two error functions defined as,

$$\text{Error}_T(\omega, n_2^*) = |T^*_{Exp,0^\circ}(\omega, n_2^*) - T^*_{Theo,0^\circ}(\omega, n_2^*)|, \quad (3)$$

$$\text{Error}_R(\omega, n_2^*) = |R^*_{Exp,45^\circ}(\omega, n_2^*) - R^*_{Theo,45^\circ}(\omega, n_2^*)|. \quad (4)$$

As defined above, these error functions can be easily calculated for a given trial value of n_2^*. After minimizing the error functions with respect to n_2^*, the real and imaginary parts of the complex optical constants n and κ ($n_2^* = n + i\kappa$) are determined for any angular frequency ω.

D. THz Conductivities and the Drude-Smith Model

Following the classical electromagnetic theory of a simple conducting medium, the equivalent complex dielectric function consisting of contributions from conduction band electrons and bound electrons can be written as [31],

$$\varepsilon^*_{\text{Equivalent}}(\omega) = \left(n_2^*\right)^2 = \varepsilon_\infty + i \cdot \sigma^*(\omega) / (\omega\varepsilon_0), \quad (5)$$

where $\varepsilon^*_{\text{Equivalent}}$ is the frequency-dependent complex dielectric constant; $\varepsilon_\infty = 4$ [31], is the high-frequency dielectric constant contributed by the bound electrons; $\varepsilon_0 = 8.854 \times 10^{-12}$ (F/m) is the free-space permittivity. The real ($\varepsilon_{\text{Re\_Equi.}}$) and imaginary ($\varepsilon_{\text{Im\_Equi.}}$) parts of equivalent dielectric constants can be expressed as,

$$\varepsilon_{\text{Re\_Equi.}} = n^2 - \kappa^2, \quad (6)$$

$$\varepsilon_{\text{Im\_Equi.}} = 2 \cdot n \cdot \kappa. \quad (7)$$

Therefore, the equivalent complex conductivity of the medium can be written in terms of the optical constants as

$$\sigma^*_{\text{Equivalent}} = 2n\kappa\omega\varepsilon_0 + i\omega\varepsilon_0(\varepsilon_\infty - n^2 + \kappa^2). \quad (8)$$

The ITO nanostructures can be considered as a mixture of ITO material and air. Previously, the simple EMA has been shown to be a useful tool for analyzing optical characteristics of the composite medium [38], [56]. In this model, the equivalent dielectric function of nanostructure can be written as,

$$\varepsilon^*_{\text{Equivalent}} = f \times \varepsilon^*_m + (1 - f) \times \varepsilon^*_h, \quad (9)$$

where ε^*_h is the dielectric constant of air; ε^*_m is the dielectric constant of pure nanostructured material. Also present in Eq. (9), f is the filling factor that defines the volume fraction of the nanostructure. For ITO NWhs with heights of 431.2 and 1387.7 nm, we estimated from Fig. 1 that $f \sim 0.18$ and ~ 0.10, respectively. Similarly, the real (ε_{Re}) and imaginary (ε_{Im}) parts of the dielectric constants of pure nanostructured material can be written as

$$\varepsilon_{\text{Re}} = [n^2 - \kappa^2 - (1 - f)]/f, \quad (10)$$

$$\varepsilon_{\text{Im}} = [2 \cdot n \cdot \kappa]/f. \quad (11)$$

Finally, the real ($\text{Re}\{\sigma\}$) and imaginary ($\text{Im}\{\sigma\}$) parts of the complex conductivities of pure ITO nanostructures can be expressed in terms of the filling factors as

$$\text{Re}\{\sigma\} = \omega\varepsilon_0 \cdot (2n\kappa)/f, \quad (12)$$

$$\text{Im}\{\sigma\} = \omega\varepsilon_0[\varepsilon_\infty - [n^2 - \kappa^2 - (1 - f)]/f]. \quad (13)$$

The Drude model was often used to analyze metals and bulk semiconductors, $\sigma^*(\omega) = \varepsilon_0\omega_p^2\tau/(1 - i\omega\tau)$ [46], where ω_p and τ are plasma frequency and scattering time of carriers in the material. The real part of conductivity, $\text{Re}\{\sigma\}$, exhibits a maximum at zero (DC) frequency, and its value decreases with increasing frequency. For $\text{Im}\{\sigma\}$, it can only be positive and approaches a maximum as the frequency approaches that of the inverse of the scattering rate [46]. As we will show in Sec. III, the THz conductivities of ITO nanostructures exhibit non-Drude-like behavior, e.g., depressed values of DC conductivity and negative values for $\text{Im}\{\sigma\}$. Therefore, the Drude-Smith model, which takes into account the carrier localization effect, is applied to fit the experimentally deduced conductivity of the ITO material [37], [57]. In this model, we write

$$\sigma^*(\omega) = \varepsilon_0\omega_p^2\tau \cdot \left[1 + \gamma / (1 - i\omega\tau)\right] / (1 - i\omega\tau), \quad (14)$$

where ω_p and τ are defined as in Eq. (13); the parameter γ is the expectation value of cosine of carrier scattering angle or the persistence of velocity of carriers. The values of γ vary from 0 to 1. The lower limit of γ, indicates Drude-like behavior or isotropic scattering of carriers. For $\gamma = -1$, we have the case of full backscattering of carriers, or strong carrier localization effect. There are some studies that attribute the non-Drude-like behavior to backscattering of carriers by grain boundaries [24], [58], [59], [65], [66]. On the other hand, the dopants in n-type TCOs will become positive ions after providing free electrons. Due to the Coulomb interaction between dopant ions and free electrons, the former will also become scattering centers hindering movement of the electrons [67], [68].

By fitting the experimentally deduced conductivities of the ITO materials by the Drude-Smith model, we can deduce the parameters ω_p and τ. The carrier concentration (N_e), mobility (μ) and DC conductivity (σ_0) can then be determined using the relations such as $N_\text{e} = \varepsilon_0\omega_\text{p}^2 m^*/e^2$, $\mu = (1+\gamma)e\tau/m^*$, and $\sigma_0 = \varepsilon_0\omega_\text{p}^2\tau\ (1+\gamma)$, respectively. In these expressions, $e = 1.602 \times 10^{-19}$ C, is the electronic charge; the electron effective mass is given by $m^* = 0.3m_0$ [69], where $m_0 = 9.1094 \times 10^{-31}$ kg, is the electron's mass.

Separating the real and imaginary part of conductivity of Eq. (14), we obtain

$$\text{Re}\{\sigma\} = \varepsilon_0\omega_p^2\tau\left[(1+\gamma)+\omega^2\tau^2(1-\gamma)\right] / \left(1+\omega^2\tau^2\right)^2, \quad (15)$$

$$\text{Im}\{\sigma\} = \varepsilon_0\omega\omega_p^2\tau^2\left(1 + 2\gamma + \omega^2\tau^2\right) / \left(1 + \omega^2\tau^2\right)^2. \quad (16)$$

Taking the derivatives of Eqs. (15) and (16), we can determine the angular frequencies at which lie the maximum value of $\text{Re}\{\sigma\}$, maximum value of $\text{Im}\{\sigma\}$ and minimum of $\text{Im}\{\sigma\}$. That is, $\omega_{\text{Re,Max}} = [-(1+3\gamma)/(1-\gamma)]^{1/2}/\tau$, $\omega_{\text{Im,Max}} = [-3\gamma + (9\gamma^2+2\gamma+1)^{1/2}]^{1/2}/\tau$, and $\omega_{\text{Im,Min}} = [-3\gamma - (9\gamma^2+2\gamma+1)^{1/2}]^{1/2}/\tau$, respecctively [48]. Similarly, the angular frequency at which $\text{Im}\{\sigma\}$ crosses zero can be written as $\omega_{\text{Im,Zero}} = (-1-2\gamma)^{1/2}/\tau$. These characteristic frequencies for extreme vlaues of $\text{Re}\{\sigma\}$ and $\text{Im}\{\sigma\}$, $\omega_{\text{Re, Max}}$, $\omega_{\text{Im,Max}}$, $\omega_{\text{Im,Min}}$ and $\omega_{\text{Im,Zero}}$, are functions of the carrier scattering time (τ) and the expectation value of cosine of scattering angle (γ). When γ is in the range of $-0.5 \sim -1.0$,

we can expect of find one maximum of Re$\{\sigma\}$, one maximum and one minimum of Im$\{\sigma\}$, respectively.

III. Results and Discussions

A. Complex THz Optical Constants of ITO Nanowhiskers and ITO Thin Films

We first investigated the transmission of THz signals through the ITO samples. Figure 5(a) and 5(b) show the waveforms of THz pulses transmitted through short ITO NWhs with height of 431.2 nm and sputtered ITO films with nearly the same thickness (440.6 nm), respectively, as well as those of the reference (bare substrate). For the analysis of complex optical constants, the time-domain THz waveforms are Fourier transformed to obtain the corresponding power spectra (see insets of Fig. 5(a) and (b)). The transmission coefficients at the peak of the THz waveforms for short and long NWhs are around 86.0% and 77.0%, respectively. In comparison, the transmission coefficients of ITO thin films of 273.4 and 440.6 nm in heights are 26.0% and 18.0%, respectively.

Figure 6(a) and 6(b) are corresponding THz-TDRS results for the same samples of ITO NWhs and thin films shown in Fig. 5 above. The reflection coefficients of THz wave incident on the short and long NWhs at AOI = 45° are ~48.0% and ~52.0%, respectively. The corresponding reflection coefficients of ITO thin films with thickness of 273.4 and 440.6 nm are ~77.0% and ~82.0%, respectively.

The frequency-dependent transmittance and reflectance of above samples are plotted in Fig. 5(c) and Fig. 6(c), respectively. In the frequency range of 0.1~1.4 THz, the transmittances of short NWhs, long NWhs, 273.4 nm-high thin film, and 440.6 nm-high thin film are ~73.0%, ~58.0%, ~7.2%, and ~3.5%, respectively.

The reflectance of above samples in the frequency range of 0.1~1.2 THz are ~24.7%, ~28.4%, ~58.8%, and ~68.3%, respectively. Comparing samples of almost the same height (short NWhs and 440.6 nm-thick thin film), our results show that the NWhs, a composite of ITO material and air, exhibit much higher transmittance (73.0/3.5 ≅ 20.9 times) and lower reflectance (24.7/68.3 ≅ 40%) than ITO thin films. The underneath basic physics is that the THz radiation can easily propagate through the air-space among NWhs. Previously, we have shown ITO NWhs exhibit broadband anti-reflection (AR) properties from the visible to the near-infrared (Reflectance ~20%) [18], [20], [48]. The data in this section show that the reflectance of ITO NWhs also reduces significantly in the THz frequency range. Such behaviors are reminiscent of broadband AR properties from UV to the far-infrared frequency range that biomimetic silicon nanotips (SiNTs) also exhibit [45].

Complex refractive indices of ITO NWhs, $n_2^* = (n + i\kappa)$, are plotted as a function of frequency in Fig. 7. These optical constants deduced from measurements by THz-TDTS and THz-TDRS are consistent. Here, the values of n_2^* are the equivalent complex refractive indices of ITO NWhs, which are treated as the mixture of air and ITO. From 0.1 to 1.6 THz, the real part of the refractive index of short NWhs decreases monotonically with frequency from 21.9 to 3.5. Similarly, n's of the samples with longer NWhs decreases from 16.0 to 4.1 in the same frequency range. The imaginary indices of refraction (κ's) of the short and long ITO NWhs, on the other hand, decrease from 19.6 to 4.5 and 12.6 to 3.6, respectively.

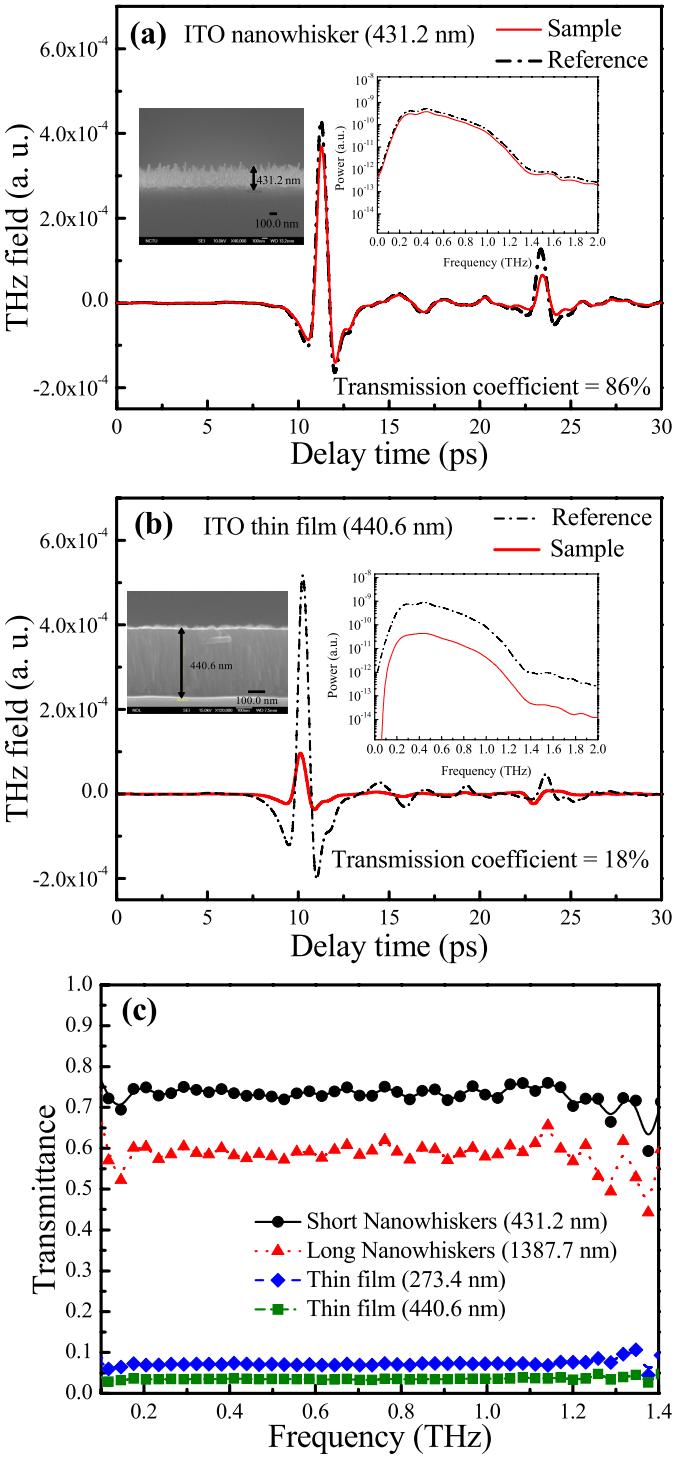

Fig. 5. Waveforms and power spectra of THz pulses transmitted normally through (a) ITO short NWhs, 431.2 nm in height, (b) ITO thin films, 440.6 nm in height. The red solid line and black dash line correspond to the signals transmitted through the sample and bare substrate, respectively. (c) Transmittance of short and long NWhs as well as ITO thin films in the frequency range of 0.1~1.4 THz.

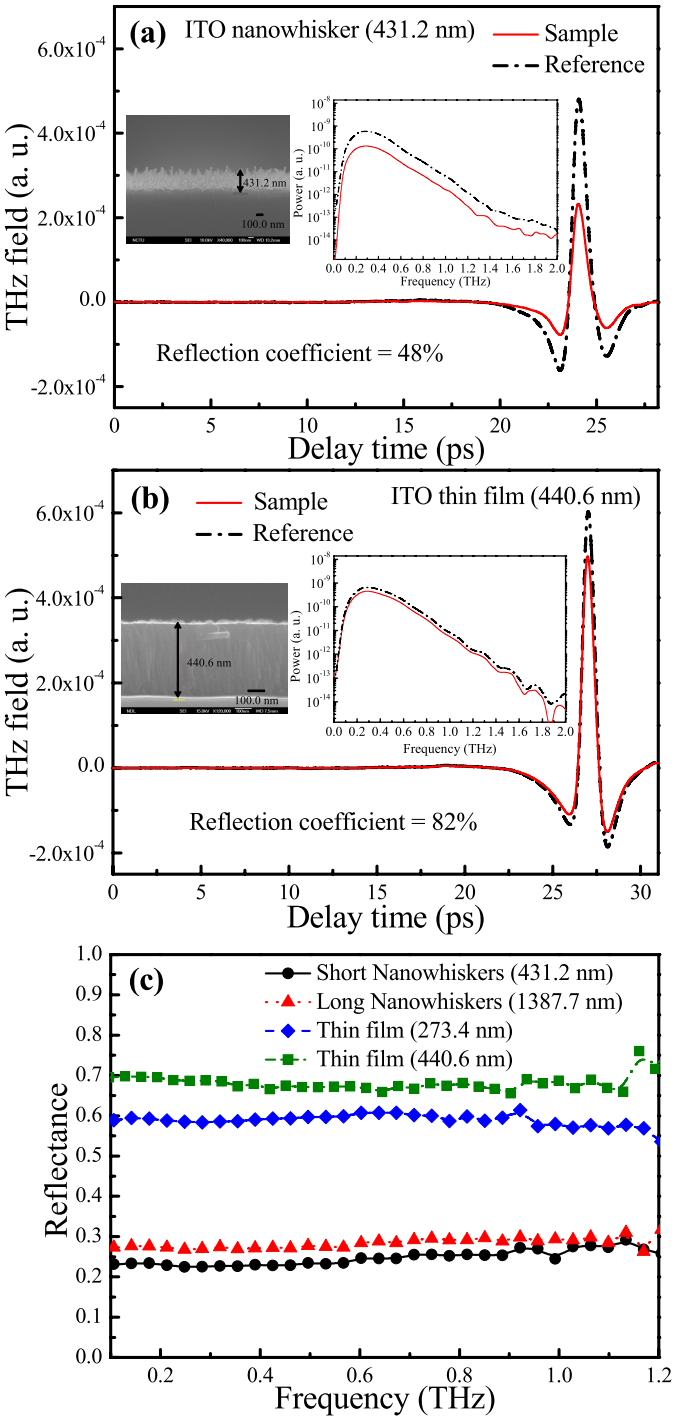

Fig. 6. Reflected waveforms and power spectra of THz pulses from (a) ITO short NWhs, height of 431.2 nm, (b) ITO thin films, thickness of 440.6 nm. The angle of the incidence (AOI) was 45°. The red solid line and black dash line correspond to the signals reflected from the sample and reference, respectively. (c) Comparison of the reflectance of short and long NWhs as well as ITO thin films in the frequency range of 0.1∼1.2 THz.

The different values of equivalent n and κ found for short and long NWhs are tentatively attributed to the difference in their volume filling factors (0.18 versus 0.10). For comparison, the complex refractive indices of ITO thin films with heights of 273.4 nm and 440.6 nm, respectively are plotted as a function of frequency in Fig. 8 (a) and 8 (b).

Note that n and κ of ITO films exhibit almost no dependence on heights. The n values decrease monotonically from

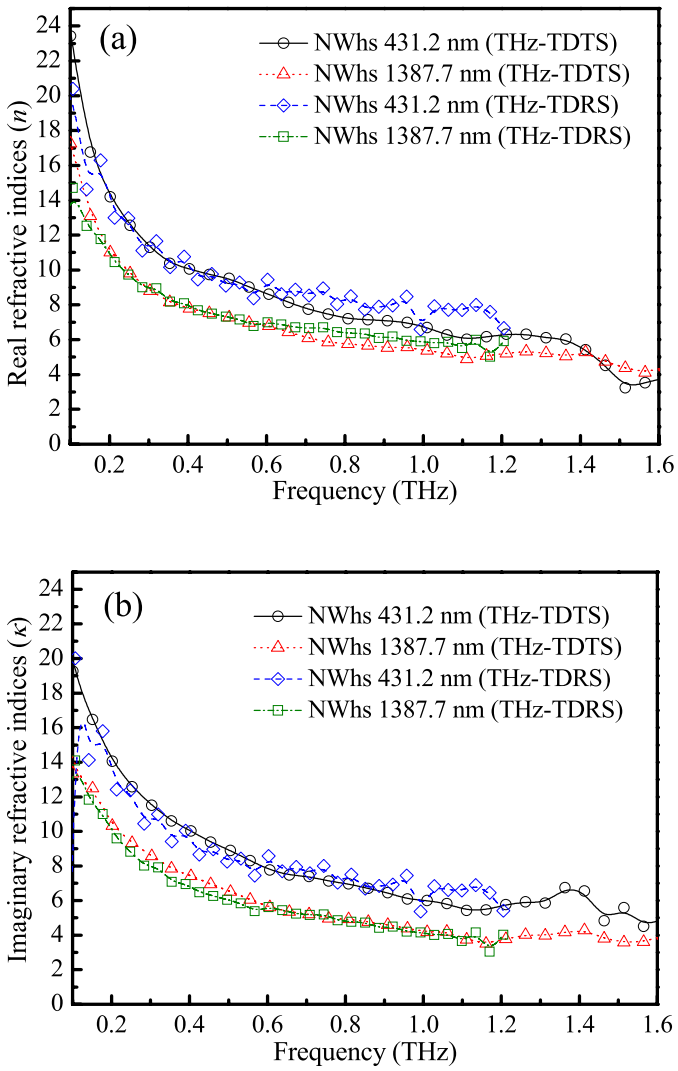

Fig. 7. (a) The real and (b) imaginary parts of the complex refractive indices of ITO NWhs with heights of 431.2 nm (short NWhs) and 1387.7 nm (long NWhs). The black circles with the solid line, red triangles with the dot line, blue diamonds with the dash line, and green squares with the dash dot line are experimental data.

80.0 to 24.0 while κ drops from 80.7 to 20.6 in the frequency range of 0.1∼1.6 THz. In general, complex optical constants of ITO thin films reported in this work are in agreement with previously reported values of Chen et al. [31] and Jewel et al. [47].

B. Electrical Characteristics of ITO Nanowhiskers and ITO Thin Films

Using Eqs. (12) and (13), we can determine the complex THz conductivities ($\sigma^* = \mathrm{Re}\{\sigma\} + \mathrm{i}\ \mathrm{Im}\{\sigma\}$) of ITO NWhs and thin films using their refractive indices. These are plotted as a function of frequency in Fig. 9 and Fig. 10, respectively.

Again, electrical parameters deduced from the THz-TDTS and THz-TDRS data are consistent (see also Table 1). For example, the values of $\mathrm{Re}\{\sigma\}$ of short and long ITO NWhs at 1.0 THz are 238 $\Omega^{-1}\mathrm{cm}^{-1}$ and 272 $\Omega^{-1}\mathrm{cm}^{-1}$, respectively. The values of $\mathrm{Re}\{\sigma\}$ for ITO NWhs increase gradually with

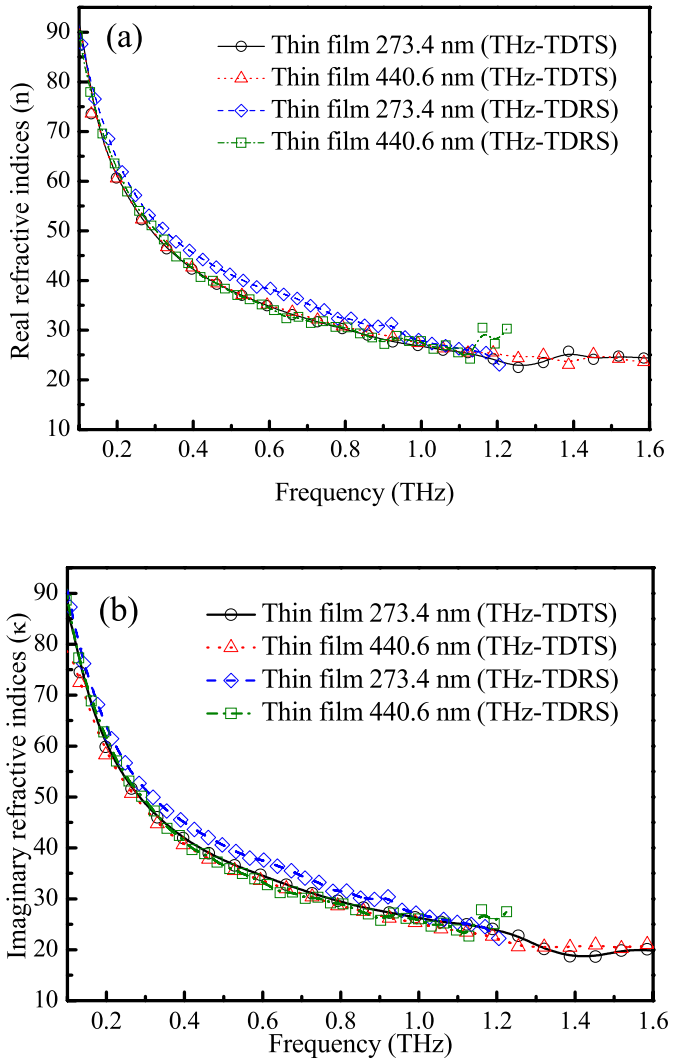

Fig. 8. The black circles with solid line, red triangles with dot line, blue diamonds with dash line, and green squares with dash dot line are (a) the real part and (b) the imaginary part of complex refractive indices of ITO thin films of two different heights using experimental data from THz-TDTS and THz-TDRS measurements.

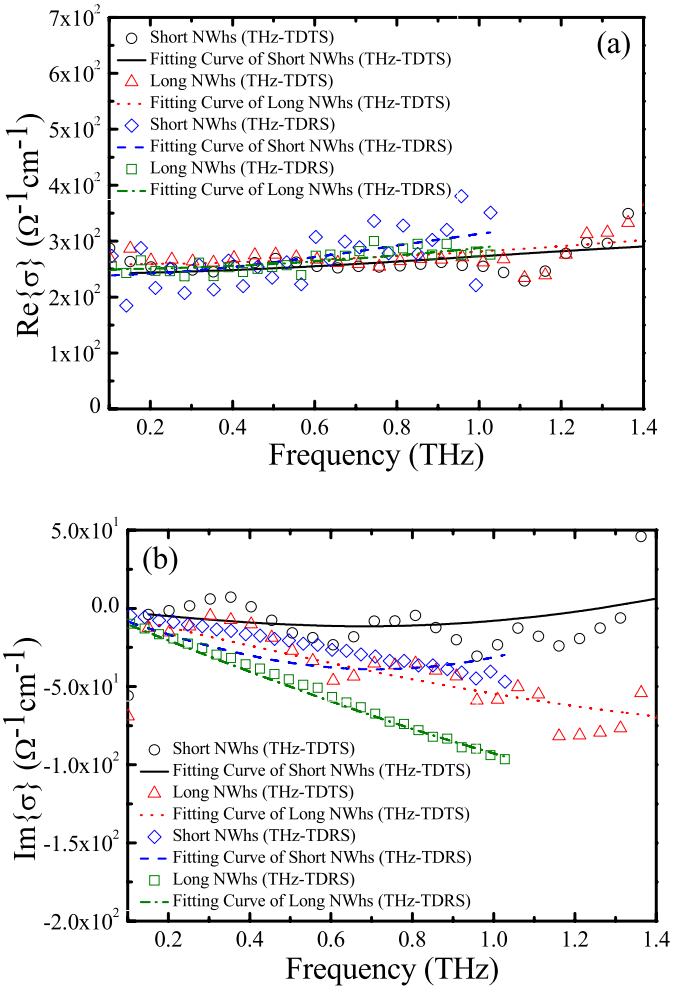

Fig. 9. (a) The real and (b) imaginary part of complex conductivities of ITO NWhs with heights of 431.2 nm (short NWhs) and 1387.7 nm (long NWhs). The black circles, red triangles, blue diamonds, and green squares are experimental data. The black solid line, red dot line, blue dash line, and green dash dot line are fitting results based on Drude-Smith model.

frequency in the range of 0.1 to 1.4 THz. On the other hand, the values of Im$\{\sigma\}$ decreases at higher THz frequencies. This trend, together with the negative values of Im$\{\sigma\}$, are generally associated with the phenomenon of carrier localization [57], [70]. This suggests that the Drude-Smith model is appropriate for modeling of complex conductivity of ITO NWhs [57]. As shown in Fig. 9(a) and 9(b), the Drude-Smith model incorporated in Eq.(14) fits THz conductivities of ITO NWhs quite well. All of the fitting parameters are summarized in Table I. For ITO short and long NWhs, the plasma frequencies are 357 versus 670 rad·THz; carrier scattering times are 57 versus 25 fs, respectively; while values of the parameter γ are around. Notably, values of γ for the two samples, -0.62 and -0.75, fall between -0.50 and -1.00. This behavior is typically associated with the presence of carrier localization in the material under study.

The mechanisms for carrier localization in ITO NWhs can be either backscattering from grain boundaries [24], [58], [59], [65], [66], or impurity ions [67], [69]. In order to determine whether anisotropic scattering of carriers by grain boundaries is important in these samples, we first evaluate the mean free path, L_{free}, which can be written as [59],

$$L_{\text{free}} = \nu_{\text{thermal}} \cdot \tau_{\text{bulk}} = \left(3 \cdot k_B \cdot T \cdot \tau_{\text{bulk}}^2 / m^*\right)^{1/2}, \quad (17)$$

where $k_{\text{B}} = 1.381 \times 10^{-23}$ J·K^{-1} is the Boltzmann constant, $T = 300$ K is the temperature in Kelvin and ν_{thermal} is the thermal velocity from classical equipartition of energy. The carrier momentum scattering time, $\tau_{\text{bulk}} = 65$ fs, is taken from our previous study of the bottom crystalline structure of ITO NWhs [48]. Using the above values, Eq. (17) yields $L_{\text{free}} \sim 13.86$ nm. To check, the carrier scattering times of ITO NWhs determined in this work are from ~25 fs to ~57 fs (See Table 1). Therefore, L_{free} of ITO NWhs, which is height-dependent, is estimated to be in the range of 5.33~12.15 nm. Alternatively, the crystal grain sizes of the orientation (222) of ITO NWhs with heights of 431.2 nm and 1387.7 nm are estimated to be 17.15 nm and 19.16 nm, respectively (see Fig. 3(a)). Similarly for the (400) peak, the corresponding crystal grain sizes of short and long ITO NWhs are estimated to be 18.02 nm and 22.19 nm, respectively. Hence, the mean

TABLE I
EXTRACTED PARAMETERS BASED ON DRUDE-SMITH MODEL OF ITO NWHS AND THIN FILMS MEASURED BY THZ-TDTS AND THZ-TDRS

ITO NWhs (THz-TDTS)						
Height (nm)	ω_p (rad·THz)	τ (fs)	γ	N_e ($\times 10^{19}$ cm^{-3})	μ (cm^{2}V^{-1}s^{-1})	σ_0 (Ω^{-1}cm^{-1})
431.2	363	49	–0.57	1.24	122	244
1387.7	648	24	–0.72	3.96	41	253
ITO NWhs, THz-TDRS						
Height (nm)	ω_p (rad·THz)	τ (fs)	γ	N_e ($\times 10^{19}$ cm^{-3})	μ (cm^{2}V^{-1}s^{-1})	σ_0 (Ω^{-1}cm^{-1})
431.2	350	64	–0.66	1.16	128	239
1387.7	691	26	–0.78	4.51	35	245
ITO thin films, THz-TDTS						
Height (nm)	ω_p (rad·THz)	τ (fs)	γ	N_e ($\times 10^{19}$ cm^{-3})	μ (cm^{2}V^{-1}s^{-1})	σ_0 (Ω^{-1}cm^{-1})
273.4	1408	13	–0.67	18.70	26	764
440.6	985	24	–0.64	9.20	51	746
ITO thin films, THz-TDRS						
Height (nm)	ω_p (rad·THz)	τ (fs)	γ	N_e ($\times 10^{19}$ cm^{-3})	μ (cm^{2}V^{-1}s^{-1})	σ_0 (Ω^{-1}cm^{-1})
273.4	1460	12	–0.59	20.10	28	933
440.6	925	26	–0.60	8.10	61	788

TABLE II
CHARACTERISTIC VALUES OF COMPLEX CONDUCTIVITIES OF ITO NWHS AND THIN FILMS MEASURED BY THZ-TDTS AND THZ-TDRS

ITO NWhs, THz-TDTS				
Height (nm)	$\omega_{Re,\,Max}/2\pi$ (THz)	$\omega_{Im,\,Max}/2\pi$ (THz)	$\omega_{Im,\,Min}/2\pi$ (THz)	$\omega_{Im,\,Zero}/2\pi$ (THz)
431.2	2.2	6.0	0.7	1.2
1387.7	5.4	13.6	2.1	4.4
ITO NWhs, THz-TDRS				
Height (nm)	$\omega_{Re,\,Max}/2\pi$ (THz)	$\omega_{Im,\,Max}/2\pi$ (THz)	$\omega_{Im,\,Min}/2\pi$ (THz)	$\omega_{Im,\,Zero}/2\pi$ (THz)
431.2	1.9	4.9	0.7	1.4
1387.7	5.3	13.0	2.1	4.6
ITO thin films, THz-TDTS				
Height (nm)	$\omega_{Re,\,Max}/2\pi$ (THz)	$\omega_{Im,\,Max}/2\pi$ (THz)	$\omega_{Im,\,Min}/2\pi$ (THz)	$\omega_{Im,\,Zero}/2\pi$ (THz)
273.4	9.5	24.2	3.6	7.0
440.6	5.0	12.8	1.8	3.5
ITO thin films, THz-TDRS				
Height (nm)	$\omega_{Re,\,Max}/2\pi$ (THz)	$\omega_{Im,\,Max}/2\pi$ (THz)	$\omega_{Im,\,Min}/2\pi$ (THz)	$\omega_{Im,\,Zero}/2\pi$ (THz)
273.4	9.2	24.7	3.0	5.6
440.6	4.3	11.5	1.5	2.7

free path is comparable to the grain size of ITO NWhs. The effect of grain boundary of ITO nanowhiskers on carrier scattering, therefore, cannot be neglected. Further, the charged impurity (Tin) scattering centers in ITO will also enhance the localization of carriers [68]. In general, the average distance between dopant ions is proportional to the inverse of the third root of doping concentration. Therefore, free electrons will run into the dopant ions easily if the doping concentration is high enough. Since the average distance between dopant ions is 2.87∼4.37 nm for ITO NWhs, free carriers can run into several scattering centers in the length of one mean free path.

Calculating from the derivatives of Re$\{\sigma\}$ (Eq.(15)) and Im$\{\sigma\}$ (Eq.(16)), we determine that $\omega_{Re,Max}/2\pi$ and $\omega_{Im,Zero}/2\pi$ of ITO short versus long NWhs are ∼2.1 THz versus ∼5.4 THz and ∼1.3 THz versus ∼4.5 THz, respectively. Besides, the $\omega_{Im,Max}/2\pi$ and $\omega_{Im,Min}/2\pi$ for NWhs samples are ∼5.5 THz versus ∼13.3 THz and ∼0.7 THz versus ∼2.1 THz, respectively. Due to the reliable frequency range of THz-TDTS (0.1∼1.4 THz) and THz-TDRS (0.1∼1.2 THz), we can only observe the frequencies of minimum ($\omega_{Im,Min}/2\pi$) and crossing zero ($\omega_{Im,Zero}/2\pi$) of Im$\{\sigma\}$, which are all around 1.0 THz. All of the characteristics values of complex conductivities are listed in the Table II. From the relations $N_e = \varepsilon_0\omega_p^2 m^*/e^2$, $\mu = (1+\gamma)e\tau/m^*$, and $\sigma_0 = \varepsilon_0\omega_p^2\tau\ (1+\gamma)$, the N_e, μ and σ_0 values of ITO NWhs with heights of 431.2 nm and 1387.7 nm are determined to be ∼1.20 versus ∼4.24 × 10^{19} cm^{-3}, ∼125 versus ∼38 cm^{2}V^{-1}s^{-1} and ∼242 versus ∼249 Ω^{-1}cm^{-1}, respectively. All of these electrical properties are summarized in Table I. We note that the DC mobility of taller sample is lower

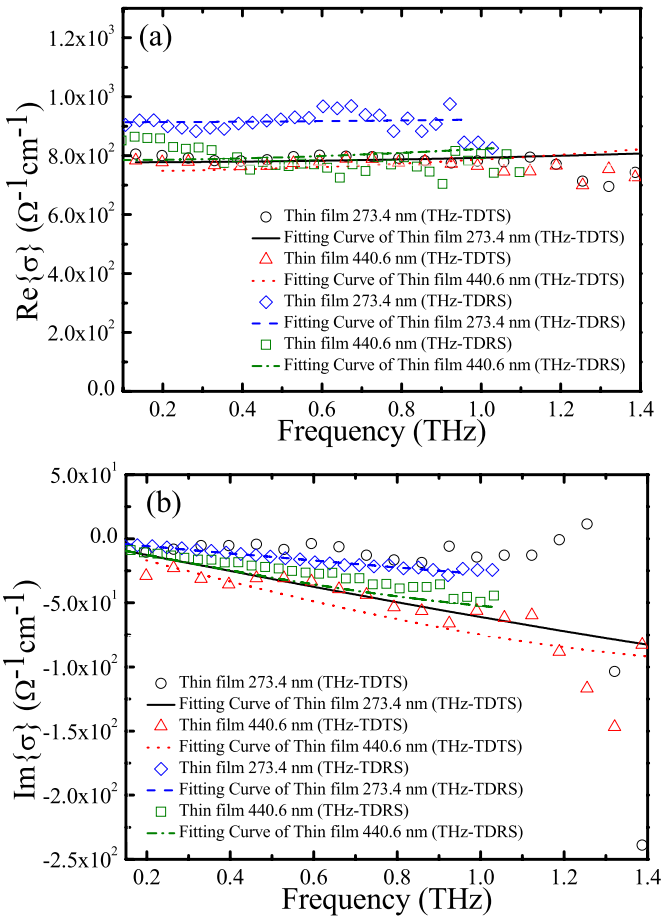

Fig. 10. (a) The real and (b) imaginary parts of complex conductivities of ITO thin films of two different heights. The black circles, red triangles, blue diamonds, and green squares are experimental data. The black-solid, red-dot, blue-dash, and green-dash dot curves are fitting results based on the Drude-Smith model.

than that of the shorter ones. These have nearly the same grain sizes (17.36 nm versus 19.40 nm). The carrier density of the former is, however, ~3.53 times higher than that of the latter. The larger density of the charged impurity ions in taller ITO NWhs means more scattering centers. This has a deterimental effect on mobility.

It is interesting to compare THz conductivities of samples studied in this work and other functional TCOs. Previous workers have shown that Tin oxide (SnO_2) NWs ($\gamma \cong -1$) [46], titanium dioxide (TiO_2) nanocrystalline ($\gamma \cong -0.93$) [36], and ZnO NWs ($\gamma \cong -0.92$) [37] all exhibit strong carrier localization. The γ values ($\gamma \cong -0.62 \sim -0.75$) of ITO NWhs are somewhat smaller than those of the other TCO nanostructures. This implies that backscattering of carriers in ITO NWs is less severe. As a consequence, mobilities of short and long ITO NWhs in this work ($38\sim 125$ $cm^2V^{-1}s^{-1}$) are higher than reported mobilities of SnO_2 NWs (~20 $cm^2V^{-1}s^{-1}$), nanocrystalline TiO_2 (1.5 $cm^2V^{-1}s^{-1}$), and ZnO NWs (~16 $cm^2V^{-1}s^{-1}$) [36], [37], [46]. The carrier concentrations of ITO NWhs ($1.20\sim4.24 \times 10^{19}$ cm^{-3}), however, are one or two orders of magnitudes higher than those found in SnO_2 NWs (8.0×10^{16} cm^{-3}), nanocrystalline TiO_2, (1.2×10^{18} cm^{-3}) and ZnO NWs (1.9×10^{18} cm^{-3}). Higher mobilities and weaker backscattering effect observed in ITO NWhs can only imply that the grain size of ITO NWhs (~19 nm) are larger than those of the nanostructrued TCOs investigated in previous works.

For comparison, the conductivities, $\mathrm{Re}\{\sigma\}$ and $\mathrm{Im}\{\sigma\}$ of ITO thin films are shown in Fig. 10(a) and 10(b), respectively. It can be seen that the frequency dependence of $\mathrm{Re}\{\sigma\}$ and $\mathrm{Im}\{\sigma\}$ of ITO films is very similar to those of ITO NWhs. As summarized in Table I, the plasma frequency, carrier scattering time and γ of 273.4 nm-high ITO thin film are ~1434 rad·THz, ~13 fs and ~ -0.63, respectively. Using these, we can calculate that N_e, μ, and σ_0 of this sample are $\sim 1.94 \times 10^{20}$ cm^{-3}, ~27 $cm^2V^{-1}s^{-1}$ and ~849 $\Omega^{-1}cm^{-1}$, respectively. These parameters for 440.6 nm-high ITO thin film are quite close (see Table I). To check, we also performed Hall measurements of the ITO thin films. It was found that N_e, μ and σ_0 of ITO thin films with heights of 273.4 nm and 440.6 nm were ~16.60 versus $\sim 4.90 \times 10^{19}$ cm^{-3}, ~39 versus ~38 $cm^2V^{-1}s^{-1}$ and ~1041 versus ~909 $\Omega^{-1}cm^{-1}$, respectively. In general, the results of Hall measurement agree with those deduced from the THz-TDS.

As shown in Fig. 10(a), $\mathrm{Re}\{\sigma\}$ of ITO thin film with thickness of 273.4 nm obtained from THz-TDRS is higher than that from THz-TDTS. Examining Eq. (1) and (2), it is clear that the accuracy in thickness of the substrate and its reference could account for the slight difference in retrieved parameters from THz-TDTS and TDRS. Here, for ITO thin films, there is no crystalline structure but strongly amorphous structures which shown in Fig. 3(b) because the farbricated method is the DC reactive magnetron sputtering Therefore, the contribution of the grain boundaries causing the carrier localization is not dominant in ITO thin films. On the other hand, regarding the localization of carriers caused by dopant ions, the average distance between each dopant ion is calculated around 1.72~2.26 nm. The carrier scattering times of ITO thin films are determined as from ~13 fs to ~25 fs. Therefore, their L_{free} are in the range of 2.77~5.33 nm, and free carriers will run into one to two in a mean free path. For the reduction of DC mobility in the sample of higher carrier concentration, it is also attributed to the larger density of scattering centers caused by the charged impurity ions.

The characteristic frequencies for extreme values of complex conductivity, $\omega_{Re,Max}/2\pi$, $\omega_{Im,Max}/2\pi$, $\omega_{Im,Min}/2\pi$, and $\omega_{Im,Zero}/2\pi$ of ITO thin films with heights of 273.4 nm and 440.6 nm are ~9.4 THz versus ~4.7 THz, ~24.5 THz versus ~12.2 THz, ~3.3 THz versus ~1.7 THz, and ~6.3 THz versus ~3.1 THz, respectively. In other words, the contribution of the plasmonic resonance is also not dominant in our measurement due to the characteristic frequencies of ITO thin films which are exceeding the reliable frequency. These are also summarized in the Table II. The main mechanism of carrier localization in the sputtered thin films is backscattering by impurity ions [37]. In comparison, the ZnO thin film shows a persistence of velocity very close -1, $\gamma \cong -0.84$ [37], much higher than that of the ITO thin film ($\gamma \cong -0.62$). This is consistent with the mobility of ZnO thin film (~40 $cm^2V^{-1}s^{-1}$) [37] is lower than that (~56 $cm^2V^{-1}s^{-1}$) of thicker ITO thin film in this work.

Comparing ITO NWhs with height of 431.2 nm (short NWhs) and thin films of nearly the same height (440.6 nm), we find their respective mobilities to be 125 $cm^2V^{-1}s^{-1}$ and 27 $cm^2V^{-1}s^{-1}$, respectively. This can be understood by noting longer carrier scattering time of the former, similar γ values for both them, and the relationship of $\mu \propto (1+\gamma) \times \tau$. Meanwhile, the carrier concentration of the ITO thin film ($\sim 8.65 \times 10^{19}$ cm^{-3}) is 7.2 times larger than that of the NWhs ($\sim 1.20 \times 10^{19}$ cm^{-3}). As a result, scattering of carriers by dopant ions is more severe in the thin films. On the other hand, we find values of the DC conductivities or real conductivities in THz region of ITO thin films (~ 800 $\Omega^{-1}cm^{-1}$) are always better than those of NWhs (~ 250 $\Omega^{-1}cm^{-1}$). This is due to larger plasma frequencies of thin films than NWhs. However, ITO NWhs exhibit transmittances ($\sim$65%) 13 times higher than those of the thin films ($\sim$5%). Reflectance of the former at AOI = 45° is also significantly lower, $\sim$42% of the latter in the THz frequency range. This can be correlated to previous reports of the broadband AR property of ITO NWhs in the visible and the THz wavelength range [48].

IV. Conclusion

In summary, we have conducted a comparative study of ITO NWhs and thin films that exhibit attractive optical and electrical properties in the THz frequency range. The ITO NWhs and thin films were fabricated by the glancing-angle electron-beam evaporation technique and DC reactive magnetron sputtering, respectively. Structural and crystalline properties of both nanostructures and thin films were examined by scanning electron microscopy and X-ray diffraction studies. By applying the Scherrer formula, the crystal grain sizes of ITO NWhs were estimated to be around 19 nm. On the other hand, ITO thin films exhibit strongly amorphous characteristics.

We employed both transmission-type and reflection-type terahertz time-domain spectroscopies (THz-TDTS and THz-TDRS) to explore the far-infrared optical and electrical properties of these samples. Key parameters, such as plasma frequencies, carrier scattering times, were analyzed and found to be fitted well by the Drude-Smith model in the 0.1$\sim$1.4 THz frequency range. The plasma frequencies of ITO NWhs with heights of 431.2 and 1387.7nm were established to be 357 and 670 rad·THz, respectively. The corresponding carrier scattering times were 57 and 25 fs, in that order. The ITO NWhs were found to exhibit much higher mobilities (38$\sim$125 $cm^2V^{-1}s^{-1}$), and weaker backscattering effect ($\gamma \cong -0.62 \sim -0.75$) than those reported for other TCO nanostructures to date. These attractive attributes are tentatively attributed to comparatively large grain size of ITO NWhs prepared this way. The carrier concentration, and DC conductivity of these two samples of ITO NWhs have also been determined to be 1.20 versus 4.24×10^{19} cm^{-3}, and 242 versus 249 $\Omega^{-1}cm^{-1}$, respectively. To compare, we have also studied ITO thin films with heights of 273.4 and 440.6 nm. The plasma frequencies of these two samples of ITO thin films were found to be 1434 versus 955 rad·THz; while the carrier scattering times were 13 versus 25 fs, respectively. Their mobilities, carrier concentrations, and DC conductivities were 27 versus 56 $cm^2V^{-1}s^{-1}$, 1.94 versus 0.87×10^{20} cm^{-3}, and 849 versus 767 $\Omega^{-1}cm^{-1}$, respectively. Significantly, we find that the complex conductivities of both ITO NWhs and thin films exhibit non-Drude-like behavior. The mechanisms that are responsible for the strong localization of carriers in ITO NWhs and thin films, however, are not exactly the same. The mean free path of ITO NWhs, 5.33$\sim$12.15 nm, approaches that of the average grain size. Their non-Drude characteristic is thus attributed to scattering of carriers at grain boundaries and backscattering by impurity ions. In contrast, observed non-Drude behavior in ITO thin films, which is amorphous, is caused by scattering of the impurity ions only.

Comparing ITO NWhs and thin films with nearly the same height, mobilities of the former is $\sim$125 $cm^2V^{-1}s^{-1}$, much larger than those of the ITO thin films, $\sim$27 $cm^2V^{-1}s^{-1}$. This is attributed to the longer carrier scattering time of the former since the γ values for both of them are nearly the same. Further, the carrier concentrations of ITO thin films were much higher than those of NWhs. The dopant ions serve as scattering centers. Nonetheless, the DC conductivities (~ 800 $\Omega^{-1}cm^{-1}$) or real conductivities in the THz frequency region of ITO thin films are higher than those of NWhs (~ 250 $\Omega^{-1}cm^{-1}$). Partly, this is a reflection of the much higher plasma frequencies of the former. This is not a problem for using ITO NWhs as electrodes except for rapid charging applications. The transmittance of ITO NWhs ($\cong$ 60$\sim$70%), however, is much higher ($\cong$ 13 times) than that of ITO thin films in the THz frequency range. The underneath basic physics is that the THz radiation can easily propagate through the air-space among NWhs. The superb transmittance and more than adequate electrical properties of ITO NWhs suggest their potential applications as transparent conducting electrodes in THz devices.

V. Acknowledgment

The authors would like to thank Prof. H.-C. Kuo for use of the electron-beam apparatus. They would also like to thank Prof. S. Gwo's group for Hall measurements. XRD was performed at the National Nanodevices Laboratories (NDL). Finally, they would like to thank Prof. C.-K. Lee for loan of the femtosecond laser system used in the THz-TDRS.

References

[1] G. J. Exarhos and X.-D. Zhou, "Discovery-based design of transparent conducting oxide films," *Thin Solid Films*, vol. 515, no. 18, pp. 7025–7052, Jun. 2007.

[2] H. Li, N. Wang, and X. Liu, "Optical and electrical properties of Vanadium doped Indium oxide thin films," *Opt. Exp.*, vol. 16, no. 1, pp. 194–199, Jan. 2008.

[3] Y.-J. Liu, C.-C. Huang, T.-Y. Chen, C.-S. Hsu, J.-K. Liou, T.-Y. Tsai, and W.-C. Liu, "Implementation of an indium-tin-oxide (ITO) direct-Ohmic contact structure on a GaN-based light emitting diode," *Opt. Exp.*, vol. 19, no. 15, pp. 14662–14670, Jul. 2011.

[4] Y.-J. Liu, C.-C. Huang, T.-Y. Chen, C.-S. Hsu, J.-K. Liou, T.-Y. Tsai, and W.-C. Liu, "On a GaN-based light-emitting diode with an indium–tin–oxide (ITO) direct-ohmic contact structure," *IEEE Photon. Technol. Lett.*, vol. 23, no. 15, pp. 1037–1049, Jul. 2011.

[5] J. W. Leem and J. S. Yu, "Glancing angle deposited ITO films for efficiency enhancement of a-Si:H/μc-Si:H tandem thin film solar cells," *Opt. Exp.*, vol. 19, no. S3, pp. A258–A268, May 2011.

[6] S. H. Lee and N. Y. Ha, "Nanostructures indium-tin-oxide films fabricated by all-solution processing for functional transparent electrodes," *Opt. Exp.*, vol. 19, no. 22, pp. 21803–21808, Oct. 2011.

[7] W.-Y. Chang, H.-J. Lin, and J.-S. Chang, "Optical panel with full multitouch using patterned indium tin oxide," *Opt. Lett.*, vol. 36, no. 6, pp. 894–896, Mar. 2011.

[8] Ö. Senlik, H. Y. Cheong, and T. Yoshie, "Design of subwavelength-size, indium tin oxide (ITO)-clad optical disk cavities with quality-factors exceeding 104," *Opt. Exp.*, vol. 19, no. 23, pp. 23469–23474, Nov. 2011.

[9] C. K. Choi, K. D. Kihm, and A. E. English, "Optoelectric biosensor using indium-tin-oxide electrodes," *Opt. Lett.*, vol. 32, no. 11, pp. 1405–1407, Jun. 2007.

[10] E. Mortazy, S. Vigne, S. Nazarpour, and M. Chaker, "Highly transparent and conductive nanometric indium tin oxide for pulse shaping applications," in *Proc. ICO Int. Conf. Inf.*, May 2011, pp. 1–2.

[11] S. Lopez, C. R. Zamarreño, M. Hernaez, I. Del Villar, F. J. Arregui, and I. R. Matias, "Optical fiber refractometers based on sputtered indium tin oxide coatings," in *Proc. 15th Int. Conf. Sens. Technol.*, Dec. 2011, pp. 585–588.

[12] D. Mergel and Z. Qiao, "Correlation of lattice distortion with optical and electrical properties of In_2O_3: Sn films," *J. Appl. Phys.*, vol. 95, no. 10, pp. 5608–5615, May 2004.

[13] J.-S. Cho, S.-K. Koh, and K. H. Yoon, "Microstructure and electrical properties of indium oxide thin films prepared by direct oxygen ion-assisted deposition," *J. Electrochem. Soc.*, vol. 147, no. 3, pp. 1065–1070, Mar. 2000.

[14] H. Kim, C. M. Gilmore, A. Pique, J. S. Horwitz, H. Mattoussi, H. Murata, Z. H. Kafafi, and D. B. Chrisey, "Electrical, optical, and structural properties of indium–tin–oxide thin films for organic light-emitting devices," *J. Appl. Phys.*, vol. 86, no. 11, pp. 6451–6461, Dec. 1999.

[15] M. M. Hamasha, K. Alzoubi, and S. Lu, "Behavior of sputtered indium–tin–oxide thin film on poly-ethylene terephthalate substrate under stretching," *J. Display Technol.*, vol. 7, no. 8, pp. 426–433, Aug. 2011.

[16] J. K. Kim, S. Chhajed, M. F. Schubert, E. F. Schubert, A. J. Fischer, M. H. Crawford, J. Cho, H. Kim, and C. Sone, "Light-extraction enhancement of GaInN light-emitting diodes by graded-refractive-index indium tin oxide anti-reflection contact," *Adv. Mater.*, vol. 20, no. 4, pp. 801–804, Feb. 2008.

[17] P. Yu, C.-H. Chang, C.-H. Chiu, C.-S. Yang, J.-C. Yu, H.-C. Kuo, S.-H. Hsu, and Y.-C. Chang, "Efficiency enhancement of GaAs photovoltaics employing antireflective indium tin oxide nanocolumns," *Adv. Mater.*, vol. 21, no. 16, pp. 1618–1621, Apr. 2009.

[18] C.-H. Chang, M.-H. Hsu, P.-C. Tseng, P. Yu, W.-L. Chang, W.-C. Sun, and W.-C. Hsu, "Enhanced angular characteristics of indium tin oxide NWhs-coated silicon solar cells," *Opt. Exp.*, vol. 19, no. S3, pp. A219–A224, May 2011.

[19] S.-P. Chiu, H.-F. Chung, Y.-H. Lin, J.-J. Kai, F.-R. Chen, and J.-J. Lin, "Four-probe electrical-transport measurements on single indium tin oxide nanowires between 1.5 and 300 K," *Nanotechnology*, vol. 20, no. 10, p. 105203, Mar. 2009.

[20] C. H. Chang, P. Yu, and C. S. Yang, "Broadband and omnidirectional antireflection from conductive indium-tin-oxide nanocolumns prepared by glancing-angle deposition with nitrogen," *Appl. Phys. Lett.*, vol. 94, no. 5, pp. 051114-1–051114-3, Feb. 2009.

[21] C.-H. Chang, P. Yu, M.-H. Hsu, P.-C. Tseng, W.-L. Chang, W.-C. Sun, W.-C. Hsu, S.-H. Hsu, and Y.-C. Chang, "Combined micro-and nanoscale surface textures for enhanced near-infrared light harvesting in silicon photovoltaics," *Nanotechnology*, vol. 22, no. 9, p. 095201, Jan. 2011.

[22] Q. Wan, Z. T. Song, S. L. Feng, and T. H. Wang, "Single-crystalline tin-ddoped indium oxide whiskers: Synthesis and characterization," *Appl. Phys. Lett.*, vol. 85, no. 20, pp. 4759–4761, Sep. 2004.

[23] A. L. Beaudry, R. T. Tucker, J. M. LaForge, M. T. Taschuk, and M. J. Brett, "Indium tin oxide NWhs morphology control by vapour-liquid-solid glancing angle deposition," *Nanotechnology*, vol. 23, p. 105608, Feb. 2012.

[24] D. G. Cooke, A. N. MacDonald, A. Hryciw, J. Wang, Q. Li, A. Meldrum, and F. A. Hegmann, "Transient terahertz conductivity in photoexcited silicon nanocrystal films," *Phys. Rev. B*, vol. 73, p. 193311, May 2006.

[25] X.-C. Zhang, and J. Xu, *Introduction to THz Wave Photonics*. New York, NY, USA: Springer-Verlag, 2010.

[26] J. Kröll, J. Darmo, and K. Unterrainer, "Metallic wave-impedance matching layers for broadband terahertz optical systems," *Opt. Exp.*, vol.15, no. 11, pp. 6552–6560, May 2007.

[27] D. G. Cooke and P. U. Jepsen, "Optical modulation of terahertz pulses in a parallel plate waveguide," *Opt. Exp.*, vol. 16, no. 19, pp. 15123–15129, Sep. 2008.

[28] K. Takase, T. Ohkubo, F. Sawada, D. Nagayama, J. Kitagawa, and Y. Kadoya, "Propagation characteristics of terahertz electrical signals on micro-strip lines made of optically transparent conductors," *Jpn. J. Appl. Phys.*, vol. 44, no. 32, pp. L1011–L1014, Jul. 2005.

[29] T. Bauer, J. S. Kolb, T. Löffler, E. Mohler, U. C. Pernisz, and H. G. Roskos, "Indium–tin–oxide-coated glass as dichroic mirror for far-infrared electromagnetic radiation," *J. Appl. Phys.*, vol. 92, no. 4, pp. 2210–2212, Aug. 2002.

[30] S. H. Brewer and S. Franzen, "Indium tin oxide plasma frequency dependence on sheet resistance and surface adlayers determined by reflectance FTIR spectroscopy," *J. Phys. Chem. B*, vol. 106, no. 50, pp. 12986–12992, Dec. 2002.

[31] C.-W. Chen, Y.-C. Lin, C.-H. Chang, P. Yu, J.-M. Shieh, and C.-L. Pan, "Frequency-dependent complex conductivities and dielectric responses of indium tin oxide thin films from the visible to the far-infrared," *IEEE J. Quantum Electron.*, vol. 46, no. 12, pp. 1746–1754, Dec. 2010.

[32] M. Walther, D. G. Cooke, C. Sherstan, M. Hajar, M. R. Freeman, and F. A. Hegmann, "Terahertz conductivity of thin gold films at the metal-insulator percolation transition," *Phys. Rev. B*, vol. 76, no. 12, pp. 125408-1–125408-9, Sep. 2007.

[33] X. H. Zhang, H. C. Guo, A. M. Yong, J. D. Ye, S. T. Tan, and X. W. Sun, "Terahertz dielectric response and optical conductivity of *n*-type single-crystal ZnO epilayers grown by metalorganic chemical vapor deposition," *J. Appl. Phys.*, vol. 107, no. 3, pp. 033101-1–033101-3, Feb. 2010.

[34] C.-W. Chen, T.-T. Tang, S.-H. Lin, J. Y. Huang, C.-S. Chang, P.-K. Chung, S.-T. Yen, and C.-L. Pan, "Optical properties and potential applications of ε-GaSe at terahertz frequencies," *J. Opt. Soc. Amer. B, Opt. Phys.*, vol. 26, no. 9, pp. A58–A65, Sep. 2009.

[35] M. C. Beard, G. M. Turner, J. E. Murphy, O. I. Micic, M. C. Hanna, A. J. Nozik, and C. A. Schmuttenmaer, "Electronic coupling in InP nanoparticle arrays," *Nano Lett.*, vol. 3, no. 12, pp. 1695–1699, Oct. 2003.

[36] G. M. Turner, M. C. Beard, and C. A. Schmuttenmaer, "Carrier localization and cooling in dye-sensitized nanocrystalline titanium dioxide," *J. Phys. Chem. B*, vol. 106, no. 45, pp. 11716–11719, Oct. 2002.

[37] J. B. Baxter and C. A. Schmuttenmaer, "Conductivity of ZnO nanowires, nanoparticles, and thin films using time-resolved terahertz spectroscopy," *J. Phys. Chem. B*, vol. 110, no. 50, pp. 25229–25239, Dec. 2006.

[38] J. Han, Z. Zhu, S. Ray, A. K. Azad, W. Zhang, M. He, S. Li, and Y. Zhao, "Optical and dielectric properties of ZnO tetrapod structures at terahertz frequencies," *Appl. Phys. Lett.*, vol. 89, no. 3, pp. 031107-1–031107-3, Jul. 2006.

[39] H. Ahn, Y.-P. Ku, Y.-C. Wang, and C.-H. Chuang, "Terahertz spectroscopic study of vertically aligned InN nanorods," *Appl. Phys. Lett.*, vol. 91, no. 16, pp. 163105-1–163105-3, Oct. 2007.

[40] A. Thoman, A. Kern, H. Helm, and M. Walther, "Nanostructured gold films as broadband terahertz antireflection coatings," *Phys. Rev. B*, vol. 77, no. 19, pp. 195405-1–195405-9, May 2008.

[41] P. Parkinson, H. J. Joyce, Q. Gao, H. H. Tan, X. Zhang, J. Zou, C. Jagadish, L. M. Herz, and M. B. Johnston, "Carrier lifetime and mobility enhancement in nearly defect-free core-shell nanowires measured using time-resolved terahertz spectroscopy," *Nano Lett.*, vol. 9, no. 9, pp. 3349–3353, Jul. 2009.

[42] N. Dawahre, J. Brewer, G. Shen, N. Harris, D. S. Wilbert, L. Butler, S. Balci, W. Baughman, S. M. Kim, and P. Kung, "Nanoscale characteristics of single crystal zinc oxide nanowires," in *Proc. 11th Int. Conf. Nanotechnol.*, Aug. 2011, pp. 640–645.

[43] F. Kernan, A. Nadarajah, J. A. Higgins, B. Pejcinovic, and R. Koenenkamp, "Terahertz characterization of zinc oxide nanowires using parallel-plate waveguides," in *Proc. 11th Int. Conf. Nanotechnol.*, Aug. 2011, pp. 404–408.

[44] P. Parkinson, C. Dodson, H. J. Joyce, K. A. Bertness, N. A. Sanford, L. M. Herz, and M. B. Johnston, "Noncontact measurement of charge carrier lifetime and mobility in GaN nanowires," *Nano Lett.*, vol. 12, no. 9, pp. 4600–4604, Aug. 2012.

[45] Y.-F. Huang, S. Chattopadhyay, Y.-J. Jen, C.-Y. Peng, T.-A. Liu, Y.-K. Hsu, C.-L. Pan, H.-C. Lo, C.-H. Hsu, Y.-H. Chang, C.-S. Lee, K.-H. Chen, and L.-C. Chen, "Improved broadband and quasi-omnidirectional anti-reflection properties with biomimetic silicon nanostructures," *Nature Nanotechnol.*, vol. 2, pp. 770–774, Dec. 2007.

[46] X. Zou, J. Luo, D. Lee, C. Cheng, D. Springer, S. K. Nair, S. A. Cheong, H. J. Fan, and E. E. M. Chia, "Temperature-dependent terahertz conductivity of tin oxide nanowire films," *J. Phys. D, Appl. Phys.*, vol. 45, no. 46, p. 465101, Oct. 2012.
[47] S. A. Jewell, E. Hendry, T. H. Isaac, and J. R. Sambles, "Tuneable Fabry–Perot etalon for terahertz radiation," *New J. Phys.*, vol. 10, p. 033012, Mar. 2008.
[48] C.-S. Yang, C. H. Chang, M.-H. Lin, P. Yu, O. Wada, and C.-L. Pan, "THz conductivities of indium-tin-oxide NWhs as a graded-refractive-index structure," *Opt. Exp.*, vol. 20, no. S4, pp. A441–A451, Jul. 2012.
[49] J. Petzelt, P. Kužel, I. Rychetský, A. Pashkin, and T. Ostapchuk, "Dielectric response of soft modes in ferroelectric thin films," *Ferroelectrics*, vol. 288, no. 1, pp. 169–185, Jan. 2003.
[50] M. Khazan, R. Meissner, and I. Wilke, "Convertible transmission-reflection time-domain terahertz spectrometer," *Rev. Sci. Instrum.*, vol. 72, no. 8, pp. 3427–3430, Aug.-2001.
[51] W.-F. Sun, X.-K. Wang, and Y. Zhang, "Measurement of refractive index for high reflectance materials with terahertz time domain reflection spectroscopy," *Chin. Phys. Lett.*, vol. 26, no. 11, p. 114210, Aug. 2009.
[52] A. Pashkin, M. Kempa, H. Němec, F. Kadlec, and P. Kužel, "Phase-sensitive time-domain terahertz reflection spectroscopy," *Rev. Sci. Instrum.*, vol. 74, no. 11, pp. 4711–4717, Nov. 2003.
[53] S. Nashima, O. Morikawa, K. Takata, and M. Hangyo, "Measurement of optical properties of highly doped silicon by terahertz time domain reflection spectroscopy," *Appl. Phys. Lett.*, vol. 79, no. 24, pp. 3923–3925, Dec. 2001.
[54] Y. C. Shen, T. Lo, P. F. Taday, B. E. Cole, W. R. Tribe, and M. C. Kemp, "Detection and identification of explosives using terahertz pulsed spectroscopic imaging," *Appl. Phys. Lett.*, vol. 86, no. 24, pp. 241116-1–241116-3, Jun. 2005.
[55] P. U. Jepsen, U. Møller, and H. Merbold, "Investigation of aqueous alcohol and sugar solutions with reflection terahertz time-domain spectroscopy," *Opt. Exp.*, vol. 15, no. 22, pp. 14717–14737, Oct. 2007.
[56] J. Han, W. Zhang, W. Chen, S. Ray, J. Zhang, M. He, A. K. Azad, and Z. Zhu, "Terahertz dielectric properties and low-frequency phonon resonances of ZnO nanostructures," *J. Phys. Chem. C*, vol. 111, no. 35, pp. 13000–13006, Jun. 2007.
[57] N. V. Smith, "Classical generalization of the Drude formula for the optical conductivity," *Phys. Rev. B*, vol. 64, no. 15, pp. 155106-1–155106-6, Oct. 2001.
[58] T. L. Cocker, L. V. Titova, S. Fourmaux, H.-C. Bandulet, D. Brassard, J.-C. Kieffer, M. A. El Khakani, and F. A. Hegmann, "Terahertz conductivity of the metal-insulator transition in a nanogranular VO_2 film," *Appl. Phys. Lett.*, vol. 97, no. 22, pp. 221905-1–221905-3, Nov. 2010.
[59] H. Němec, P. Kužel, and V. Sundström, "Far-infrared response of free charge carriers localized in semiconductor nanoparticles," *Phys. Rev. B*, vol. 79, no. 11, pp. 115309-1–115309-7, Mar. 2009.
[60] A. L. Patterson, "The Scherrer formula for X-Ray particle size determination," *Phys. Rev.*, vol. 56, no. 10, pp. 978–982, Jul. 1939.
[61] R.-P. Pan, C.-F. Hsieh, C.-L. Pan, and C.-Y. Chen, "Temperature-dependent optical constants and birefringence of nematic liquid crystal 5CB in the terahertz frequency range," *J. Appl. Phys.*, vol. 103, no. 9, pp. 093523-1–093523-7, May. 2008.
[62] C.-S. Yang, C.-J. Lin, R.-P. Pan, C. T. Que, K. Yamamoto, M. Tani, and C.-L. Pan, "The complex refractive indices of the liquid crystal mixture E7 in the terahertz frequency range," *J. Opt. Soc. Amer. B*, vol. 27, no. 9, pp. 1866–1873, Sep. 2010.
[63] C.-K. Lee, C.-S. Yang, S.-H. Lin, S.-H. Huang, O. Wada, and C.-L. Pan, "Effects of two-photon absorption on terahertz radiation generated by femtosecond-laser excited photoconductive antennas," *Opt. Exp.*, vol. 19, no. 24, pp. 23689–23697, Nov. 2011.
[64] M.-H. Lin, "Terahertz reflection spectroscopic studies of the optical and electrical properties of indium-tin-oxide thin films and NWhs," M.S. thesis, Dept. Phys., Nat. Tsing Hua Univ., Hsinchu, Taiwan, 2011.
[65] H. Němec, P. Kužel, and V. Sundström, "Charge transport in nanostructured materials for solar energy conversion studied by time-resolved terahertz spectroscopy," *J. Photochem. Photobiol. A Chem.*, vol. 215, nos. 2–3, pp. 123–139, Aug. 2010.
[66] L. V. Titova, T. L. Cocker, D. G. Cooke, X. Wang, A. Meldrum, and F. A. Hegmann, "Ultrafast percolative transport dynamics in silicon nanocrystal films," *Phys. Rev. B*, vol. 83, no. 8, pp. 085403-1–085403-9, Feb. 2011.
[67] E. Conwell and V. F. Weisskopf, "Theory of impurity scattering in semiconductor," *Phys. Rev.*, vol. 77, no. 3, pp. 388–390, Feb. 1950.
[68] J. Ederth, "Electrical transport in nanoparticle thin films of gold and indium tin oxide," Ph.D. dissertation, Dept. Mater. Sci., Uppsala Univ., Uppsala, Sweden, 2003.
[69] J. Gao, R. Chen, D. H. Lin, L. Jiang, J. C. Ye, X. C. Ma, X. D. Chen, Q. H. Xiong, H. D. Sun, and T. Wu, "UV light emitting transparent conducting tin-doped indium oxide (ITO) nanowires," *Nanotechnology*, vol. 22, no. 19, p. 195706, May 2011.
[70] T.-T. Kang, M. Yamamoto, M. Tanaka, A. Hashimoto, A. Yamamoto, R. Sudo, A. Noda, D. W. Liu, and K. Yamamoto, "Terahertz characterization of semiconductor alloy AlInN: Negative imaginary conductivity and its meaning," *Opt. Lett.*, vol. 34, no. 16, pp. 2507–2509, Aug. 2009.

Chan-Shan Yang received the master's (M.S.) degree in electro-optical engineering from the Department of Photonics and Institute of Electro-Optical Engineering, National Chiao-Tung University, Hsinchu, Taiwan, in 2009. He is currently pursuing the Ph.D. degree in physics with the Department of Physics, National Tsing Hua University, Hsinchu. His current research interests include ultrafast optics, terahertz photonics and optoelectronic material in the THz band.

Mao-Hsiang Lin received the master's (M.S.) degree in physics from the Department of Physics, National Tsing Hua University, Hsinchu, Taiwan, in 2011. His current research interests include terahertz photonics.

Chia-Hua Chang was born in Taipei, Taiwan, in 1983. He received the B.S. degree in materials science and engineering and the M.S. degree in electro-optical engineering from National Chiao-Tung University, Hsinchu, Taiwan, in 2006 and 2009, respectively, where he is currently pursuing the Doctoral degree with the Institute of Electro-Optical Engineering. His current research interests include the fabrication and simulation of indium-tin-oxide nanostructures on light-emitting devices and solar cell.

Peichen Yu (M'06) was born in Taipei, Taiwan, in 1974. She received the B.S. degree in electrophysics and the M.S. degree in electro-optical engineering from National Chiao-Tung University, Hsinchu, Taiwan, in 1996 and 1998, respectively, and the Ph.D. degree in electrical engineering from the University of Michigan, Ann Arbor, MI, USA, in 2004. From 2004 to 2006, she was a RET Design Engineer for the Advanced Design Group, Intel Corporation, Hillsboro, OR, USA. In 2006, she joined the Department of Photonics, Institute of Electro-Optical Engineering, National Chiao-Tung University, as an Assistant Professor and an Associate Professor in August 2009. Her current research interests include the design and development of nanostructured solar cells, light emitting diodes, and silicon-based nano-devices. She is actively engaged in the development of OPC and DFM solutions for CMOS 32 nm microlithography. She is a member of the IEEE Photonics Society and SPIE.

Jia-Min Shieh received the Ph.D. degree in electro-optics from National Chiao-Tung University, Hsinchu, Taiwan, in 1997. Currently, he is a Researcher with National Nano Device Laboratories, Hsinchu, and leads the photovoltaic/photonic device division in NDL. His current research interests include photovoltaic/photonic devices and nanoelectronics. His research focuses on developing Si and CIGS thin-film solar cells, solar self-powered electronics, and stacked 3-D electronics.

Chang-Hong Shen received the Ph.D. degree in physics from National Tsing-Hua University, Hsinchu, Taiwan, in 2006. Currently, he is an Associate Researcher with National Nano Device Laboratories, Hsinchu. His current research interests include developing Si and CIGS thin-film solar cells and solar self-powered electronics.

Osamu Wada (S'70–M'72–SM'93–F'97) received the B.E. degree from the Himeji Institute of Technology, Himeji, Japan, and the M.E. degree from Kobe University, Kobe, Japan, both in electrical engineering, and the Ph.D. degree in electronic and electrical engineering from the University of Sheffield, Sheffield, U.K. In 1971, he joined Fujitsu Laboratories Ltd., Kawasaki, Japan. From 1971 to 1976, he was engaged in research on Gunn-effect logic ICs. From 1976 to 1978, he was an Independent Researcher, supported by the Science Research Council, U.K., the University of Sheffield, for research on InP materials and devices. Since 1978, he has been engaged in research on various optoelectronic devices, including InP-based LEDs, p-i-n photodiodes (p-i-nPDs), and avalanche photodiodes, and optoelectronic ICs (OEICs) on both GaAs and InP material systems for the application to optical communications and optical interconnections. From 1989 to 1996, he was a Research Fellow with Atsugi Laboratory, Fujitsu Laboratories Ltd., Atsugi, Japan. In 1996, he was a Group Leader with the Femtosecond Technology Research Association, Tsukuba, Japan, for the METI/NEDO project on Femtosecond Technology, in-charge of research on ultrafast all-optical switching devices. In 2001, he joined a Professor in the Department of Electrical and Electronics Engineering, Kobe University, Kobe, where he has been the Director of the Division of Frontier Research and Technology, Center for Collaborative Research and Technology Development since 2003. His current research interests include quantum dots and III–V semiconductor materials and their applications to photonic devices. He is currently a Visiting Professor with CREATE, Kobe University, and a Senior Advisor of Japan Society of Applied Physics. He is a fellow of the Optical Society of America, The Institute of Electronics, Information and Communication, and the Japan Society of Applied Physics.

Ci-Ling Pan (M'88–SM'03–F'12) is a Tsing Hua Chair Professor and a Chairperson of the Department of Physics and Institute of Astronomy, National Tsing Hua University (NTHU), Hsinchu, Taiwan. He held joint appointment with the Institute of Photonics Technologies and served as the Director of the Photonics Research Center of NTHU. He was with National Chiao-Tung University, Hsinchu, from 1981 to 2009. He held visiting professorship with Osaka University, Osaka, Japan, and Chinese University of Hong Kong, Hong Kong, in 2004 and 2008, respectively. His research focuses on ultrafast and THz photonics. His current research interests include the developments of functional liquid crystal THz photonic devices, femtosecond-laser recrystallization and activation of silicon as well as novel THz generators and detectors. The latter have been used in diverse applications, such as diagnostics of technologically important materials for photovoltaics, assessing burn trauma and optical-network-compatible W-band (100 GHz or 0.1 THz) wireless communication Link at a data rate beyond 20 Gbit/s. He is a fellow of APS, OSA, and SPIE.